

Spin triplet exciton condensations in LaCoO₃ at ultrahigh magnetic fields up to 600 T

Akihiko Ikeda,^{1,2,*} Yasuhiro H. Matsuda,¹ Keisuke Sato,³ Yuto Ishii,¹
 Hironobu Sawabe,¹ Daisuke Nakamura,¹ Shojiro Takeyama,¹ and Joji Nasu^{4,5}

¹Institute for Solid State Physics, University of Tokyo, Kashiwa, Chiba 277-8581, Japan

²Department of Engineering Science, University of Electro-Communications, Chofu, Tokyo 182-8585, Japan

³National Institute of Technology, Ibaraki College, Hitachinaka, Ibaraki 312-0011, Japan

⁴Department of Physics, Tohoku University, Sendai, Miyagi 980-8578, Japan

⁵PRESTO, Japan Science and Technology Agency, Honcho Kawaguchi, Saitama 332-0012, Japan

(Dated: January 11, 2022)

Bose-Einstein condensation of electron hole pairs, exciton condensation, has been effortfully investigated since predicted 60 years ago [1, 2]. Irrefutable evidence has still been lacking due to experimental difficulties in verifying the condensation of the charge neutral and non-magnetic spin-singlet excitons [3–7]. Whilst, condensation of spin-triplet excitons is a promising frontier because the spin supercurrent [8, 9], spin-Seebeck effects [10] will be observable. A canonical cobaltite LaCoO₃ under very high magnetic fields is a propitious candidate, yet to be verified [11–15]. Here, we unveil the exotic phase diagram of LaCoO₃ up to 600 T generated using the electromagnetic flux compression method [16] and the state-of-the-art magnetostriction gauge [17]. We found successive emergence of two spin-triplet exciton condensates identified by the gapless magnetostriction curves and model calculations. The spin-triplet exciton condensation in a cobaltite, that is three dimensional and thermally equilibrated, opens up a novel venue for spintronics technologies with spin-supercurrent such as a spin Josephson

junction.

Novel phases in condensed matters often emerge at the boundaries of incompatible phases aided by the competing interactions, fluctuations and spontaneous symmetry breakings. Insulating state by a Bose-Einstein condensation of electron-hole pairs, excitonic insulator or exciton condensation, has been eagerly investigated for over 50 years since the prediction [2] at the boundary region between semi-metals and semi-conductors and their photo-excited states. However, compelling evidence has been lacking, due to the difficulty in verifying the condensation of charge neutral and spin-singlet excitons [3–7].

On the other hand, the condensation of the spin-triplet excitons is more beneficial to investigate thanks to observable magnetic phenomena such as spin-supercurrent [8, 9] and spin Seebeck effect [10], which are attractive for potential appli-

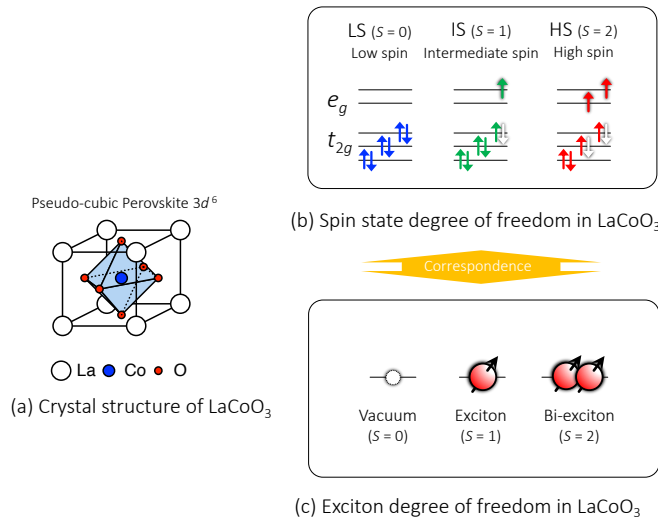


FIG. 1. Schematic drawings of (a) crystal structure, (b) spin-state degrees of freedom, (c) and corresponding excitonic degrees of freedom in LaCoO₃. LS and a pair of shaded electron and hole in (b) correspond to vacuum and an exciton in (c), respectively.

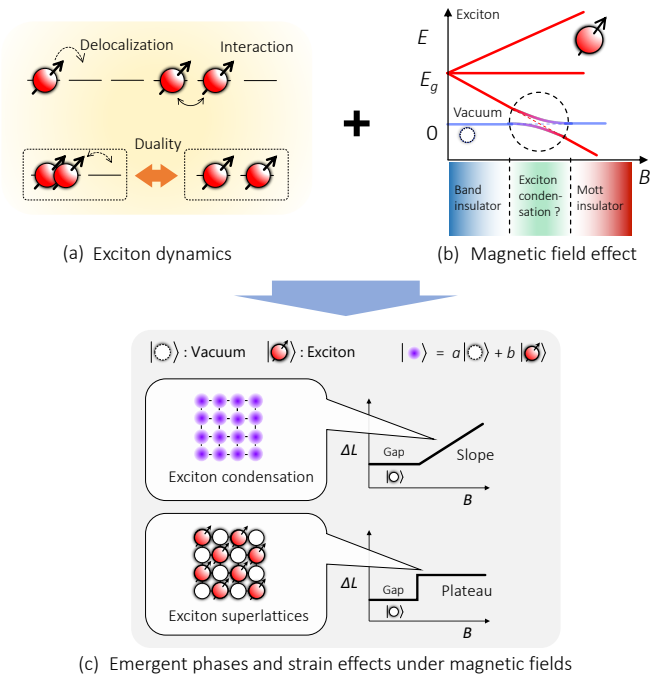


FIG. 2. Schematics drawings of (a) the interactions and dynamics of the excitons, and (b) the magnetic field effect on the exciton states in LaCoO₃. (c) Expected emergence of the magnetic field induced phases in LaCoO₃, and the resultant magnetostriction curves.

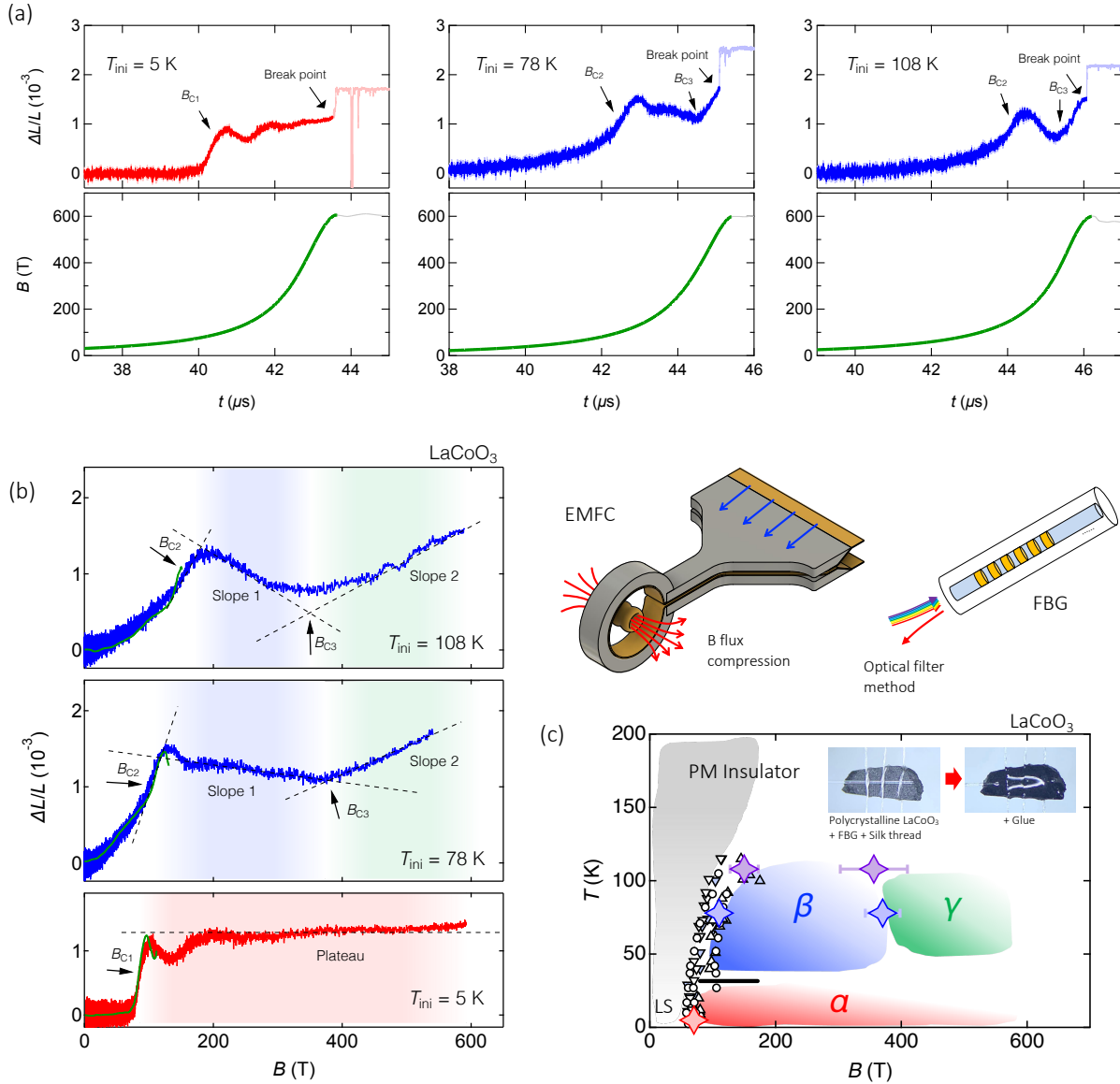


FIG. 3. Magnetostriction data of $LaCoO_3$ (a) as a function of time at various initial temperatures along with the magnetic field profile generated using the electromagnetic flux compression method, and (b) those as a function of magnetic field at various temperatures, along with the previous data (Green curves) using STC in Ref. [18]. (c) Summary of the magnetostriction measurement of $LaCoO_3$ on a magnetic field-temperature plane up to 600 T along with the previously obtained data using magnetization [19] and magnetostriction measurements [18].

cations in spintronics and quantum computing technologies. Condensation of spin-triplet bosons is of a fundamental interest in analogy with the spin-triplet superconductivity [20, 21] and superfluidity of 3He [22]. The condensation of spin-triplet excitons has been rarely considered in conventional studies of exciton condensations [3–7].

Recently, theories have predicted that spin-triplet exciton condensation is stable in perovskite cobaltites with strongly correlated electrons [11–13]. This is based on the fact that the spin-state degrees of freedom are inherent in the cobaltites [see Fig. 1(a) and 1(b)] due to the competing Hund’s coupling and the crystal field splitting, which can also be viewed as the novel

degrees of freedom of atomic size excitons [see Fig. 1(c)]. The spin-triplet exciton condensation is essentially the quantum hybridization of the distinct exciton states. The hybridization is due to the delocalization, interaction, and duality of excitons [see Fig. 2(a)] that are promoted when the energies of the vacuum and exciton states are in proximity by such external fields as magnetic fields. The LS and HS states correspond to the Mott insulator and the band insulator phases, respectively [11]. Thereby, the spin-triplet exciton condensation occurs at the boundary region between the incompatible phases [See Fig. 2(b)]. Note that it is also a multipole order of spin and orbital degrees of freedom [23].

A doped perovskite cobaltite $\text{Pr}_{0.5}\text{Ca}_{0.5}\text{CoO}_3$ and its family compounds are the first candidate for the spin-triplet excitonic condensation, exhibiting an insulating and paramagnetic ground phase at low temperatures [24, 25]. The origin of the insulator phase is, however, not completely uncovered because the significant valence transition of Pr complicates the phase transition. Next, the most well-known cobaltite LaCoO_3 has been claimed to be a promising candidate when placed under very high magnetic fields exceeding 100 T [14, 15]. LaCoO_3 has a variety of spin-states, such as low-spin (LS: $S = 0, t_{2g}^6 e_g^0$), intermediate spin (IS: $S = 1, t_{2g}^5 e_g^1$) and high spin (IS: $S = 2, t_{2g}^4 e_g^2$) states [See Fig. 1(b)], which are viewed as exciton states of vacuum, single exciton and bi-exciton, respectively [See Fig. 1(c)]. The spin-triplet excitonic condensation will emerge when the magnetic field eliminates the spin gap and changes the vacuum state (LS) to a magnetic single exciton state (IS) or bi-exciton states (HS) [See Fig. 2(b)].

However, the experimental investigation has been challenging due to the need for very high magnetic fields beyond 100 T necessitated by the large spin-gap of ~ 100 K, and also the need for the probe of the exciton states at such high fields. Recently, we reported the generation of 1200 T with electromagnetic flux compression (EMFC) method using a newly installed discharge capacitor banks in ISSP [16]. Besides, we succeeded in implementing a state-of-the-art high-speed 100 MHz strain gauge using fiber Bragg grating (FBG) and optical filter method [17], which have enabled us to measure magnetostriction in the μs -pulsed 1000 T environment. Magnetostriction is a crucial probe of the exciton states because the density of excitons is coupled to the lattice volume of LaCoO_3 . As indicated in Refs. [14, 15, 26], the plateaux and slopes in the magnetostriction correspond to solidifications and Bose-Einstein condensation of excitons in LaCoO_3 , respectively [See Fig. 2(c)]. Note that the correspondences are analogues to the magnetization plateaux and slopes in magnon solids and superfluids, respectively [27, 28].

Previously in LaCoO_3 , the field induced phase transitions are uncovered below 30 K (α phase) [29–31] and above 30 K (β phase), which extend beyond 100 T, using magnetization and magnetostriction measurements up to 200 T generated by single turn coil (STC) method [18, 19]. The two phases are considered superlattice formation of the single excitons, bi-excitons, and vacuum based on the plateaux of magnetostrictions. Considering that the spin-state and magnetization below 200 T being far from the full polarization, further orderings of excitons are expected to appear at above 200 T. Now, we are fully equipped for the investigation of the evolution of the excitonic states in LaCoO_3 beyond 200 T.

Figs. 3(a)-3(c) and shows the results of longitudinal magnetostriction measurements of polycrystalline LaCoO_3 up to 600 T with the initial sample temperatures $T_{\text{ini}} = 5, 78, \text{ and } 108$ K. Fig. 3(a) and 3(b) shows the magnetostriction data as functions of time and magnetic fields, respectively. The magnetostriction data up to 150 T in Ref. [18] are shown for comparison using green curves in Fig. 3(b). The transition

points are indicated in 3(b) and summarized using star shaped symbols in Fig. 3(c) along with the previous results up to 150 T [18, 19] shown using filled and open triangle and squares. The transitions and features below 200 T well reproduce the previous observations up to 150 T [See Fig. 3(b)] where the transition fields are denoted as B_{C1} and B_{C2} . In Fig. 3(a), the propagation of a shock wave inside the sample initiated by the strong transitions of B_{C1} and B_{C2} are present [18, 32, 33]. The temperature changes of the sample during the application of the $\mu\text{-second}$ pulsed magnetic field are considered significant at $T_{\text{ini}} = 5$ K, while it is negligible at $T_{\text{ini}} > 30$ K based on the sufficiently large heat capacity above 30 K [34] and a preliminary measurement of magnetocaloric effects up to 65 T [35].

We found that the magnetostriction plateau of α phase at $T_{\text{ini}} = 5$ K that appears at 70 T persists up to 600 T, revealing the significant stability under magnetic fields. On the other hand, β phase has been found to show a negative slope of magnetostriction [See slope 1 in Fig. 3(b)] between 170 T and 380 T. Further, we found a new phase transition at 380 T denoted as B_{C3} from β phase to a novel state in the data at $T_{\text{ini}} = 78$ K, which we term γ phase, being characterized with a positive slope beyond 380 T [See slope 2 in Fig. 3(b)]. Previously in Ref. [18], β phase was falsely considered a plateau due to the limited measurement regions below 200 T. We note that the sharpness of the transition at B_{C3} is lost with increasing temperature at $T_{\text{ini}} = 108$ K data, implying that the upper boundary of γ phase is located at ~ 100 K.

Here, we discuss the origins of $\alpha, \beta,$ and γ phases in LaCoO_3 induced at ultrahigh magnetic fields. We claim that α phase is a superlattice of spin-triplet excitons and vacuum, based on the present observation of the magnetostriction plateau at 5 K shown in Fig. 3(a) and that the magnetization of α phase is only 1/8 or 1/4 of the saturation excitons [29, 30]. In the exciton superlattice, the number of exciton is discrete [13], leading to the magnetostriction plateau as is shown in the data at 5 K in Fig. 3(a). This is in good agreement with the previous observations and considerations on α phase [18, 29–31]. The remarkable stability of α phase that sustains up to 600 T suggests the localized nature of the spin-triplet excitons in α phase of LaCoO_3 .

On the other hand, β and γ phases show gapless magnetostriction slopes denoted as slope 1 and slope 2 in Figs. 3(d), which indicate that exciton density varies continuously as a function of magnetic fields. These gapless behaviors evoke the Bose-Einstein condensation of spin-triplet excitons. In a condensate of excitons, the single site wave function of Co is described by $|\phi_{\text{EC}}\rangle = a|0\rangle + b|1\rangle + c|2\rangle$, where $|0\rangle, |1\rangle, |2\rangle$ represents the vacuum, a single-exciton and a bi-exciton occupied states, respectively, with a global wave-function of $|\psi_{\text{EC}}\rangle = \prod_i |\phi_{\text{EC}}\rangle_i$. The continuous change of magnetostriction and magnetization is realized because the coefficients a, b, c change continuously in exciton condensates as a function of magnetic field [14, 15]. A possible origin of the continuous magnetostriction is thermal activation, which is ruled out by the negative magnetostriction slopes as shown in Fig. 3(d).

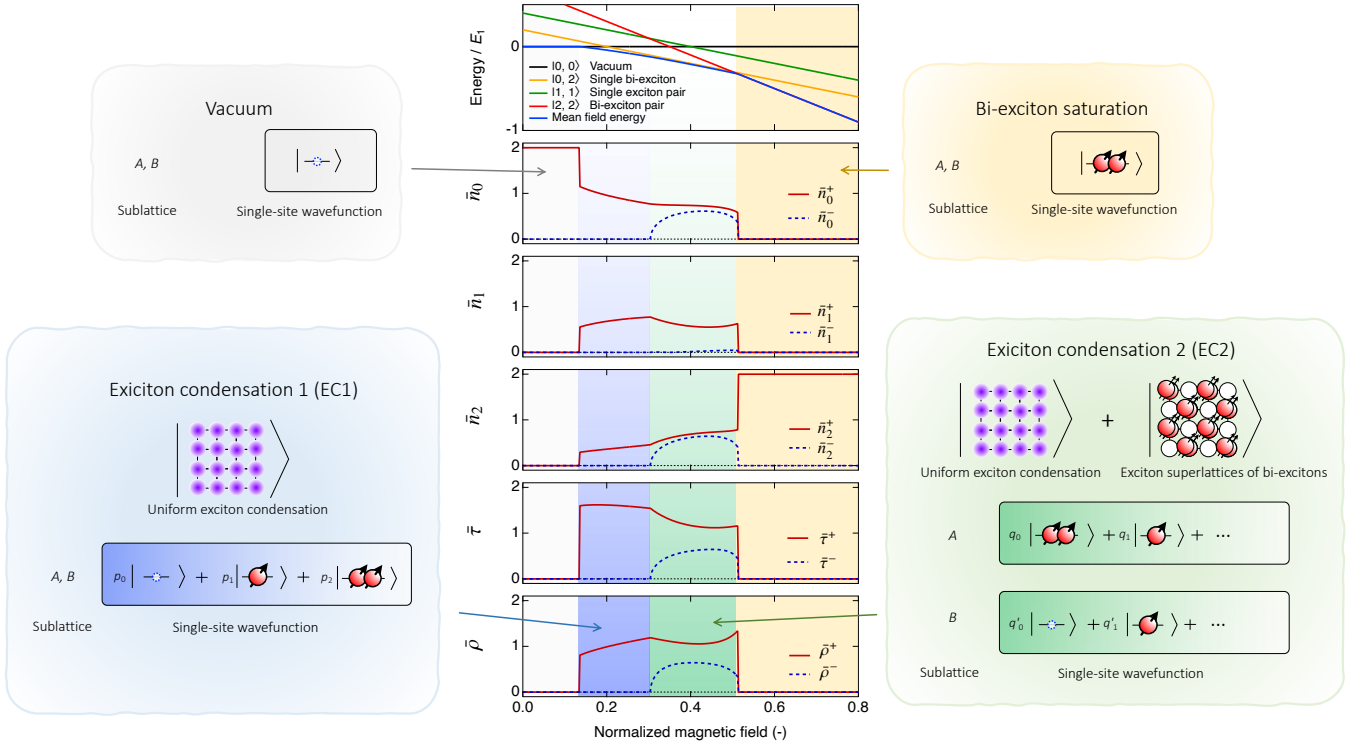


FIG. 4. The calculated results of the proposed model of the excitonic states of LaCoO_3 under ultrahigh magnetic field. The parameters are chosen to be $(E_1, E_2, J_{11}, J_{02}, t, V, g_1, g_2) = (1.0, 0.7, 0.2, 0.05, 0.07, 0.17, 1, 2)$. See main text and the Supplemental Material for more details.

Another possibility, orbital order, is also ruled out as the main cause of the present result because polycrystalline samples are used and LaCoO_3 is a mostly isotropic pseudo-cubic system [36].

For considering the condensation of spin-triple exciton condensation in LaCoO_3 at ultrahigh magnetic fields, we tentatively construct a phenomenological model and analyze it using the mean-field theory with the A, B sublattices. In the presence of strong magnetic field, the model Hamiltonian is constructed as,

$$\mathcal{H} = \mathcal{H}_{\text{loc}} + \mathcal{H}_{\text{int}} + \mathcal{H}_{\text{trans}} + \mathcal{H}_{\text{dual}}. \quad (1)$$

Each terms are expressed as

$$\mathcal{H}_{\text{loc}} = (E_2 - g_2 h) \sum_i n_i^{(2)} + (E_1 - g_1 h) \sum_i n_i^{(1)}, \quad (2)$$

$$\mathcal{H}_{\text{int}} = -J_{11} \sum_{\langle ij \rangle} n_i^{(1)} n_j^{(1)} - J_{02} \sum_{\langle ij \rangle} (n_i^{(2)} n_j^{(0)} + n_i^{(0)} n_j^{(2)}), \quad (3)$$

$$\mathcal{H}_{\text{trans}} = -t \sum_{\langle ij \rangle} (|0, 1\rangle_{ij} \langle 1, 0|_{ij} + |1, 0\rangle_{ij} \langle 0, 1|_{ij}), \quad (4)$$

$$\mathcal{H}_{\text{dual}} = -V \sum_{\langle ij \rangle} \left(|1, 1\rangle_{ij} \left(\langle 2, 0|_{ij} + \langle 0, 2|_{ij} \right) \right. \quad (5)$$

$$\left. + \left(|2, 0\rangle_{ij} + |0, 2\rangle_{ij} \right) \langle 1, 1|_{ij} \right), \quad (6)$$

where, for simplicity, only three states $\{|0\rangle, |1\rangle, |2\rangle\}$ are considered as the local bases [37]. The local term \mathcal{H}_{loc} defines the energy of each exciton state at magnetic fields h . E_k , g_k , and $n_i^{(k)}$ with $k = 0, 1, 2$ are the energy, effective g -factor and number operator of $|k\rangle_i$ excitonic states. The interaction term \mathcal{H}_{int} describes the attractive interactions J_{11} , J_{02} between neighboring excitons as $|1, 1\rangle_{ij}$ and $|0, 2\rangle_{ij}$, respectively, where $\langle ij \rangle$ represents the nearest neighbor pair. The transfer term $\mathcal{H}_{\text{trans}}$ describes the delocalization of single exciton states as $|0, 1\rangle_{ij} \rightleftharpoons |1, 0\rangle_{ij}$. The duality term $\mathcal{H}_{\text{dual}}$ hybridizes the neighboring pair $|2, 0\rangle_{ij}$ and the pair $|1, 1\rangle_{ij}$ as $|2, 0\rangle_{ij} \rightleftharpoons |1, 1\rangle_{ij}$, which describes the duality of a $|2\rangle$ state and two $|1\rangle$ states [38, 39]. The order parameters of the excitonic condensations are defined as $\langle \tau \rangle$ and $\langle \rho \rangle$, where $\tau_i^x = |0\rangle_i \langle 1|_i + \text{H.c.}$, $\tau_i^y = i|0\rangle_i \langle 1|_i + \text{H.c.}$, $\rho_i^x = |1\rangle_i \langle 2|_i + \text{H.c.}$, and $\rho_i^y = i|1\rangle_i \langle 2|_i + \text{H.c.}$, respectively. We further define $\bar{n}_k^\pm = |\langle n^{(k)} \rangle_A \pm \langle n^{(k)} \rangle_B|$, $\bar{\tau}^\pm = \sqrt{(\langle \tau^x \rangle_A \pm \langle \tau^x \rangle_B)^2 + (\langle \tau^y \rangle_A \pm \langle \tau^y \rangle_B)^2}$, and $\bar{\rho}^\pm = \sqrt{(\langle \rho^x \rangle_A \pm \langle \rho^x \rangle_B)^2 + (\langle \rho^y \rangle_A \pm \langle \rho^y \rangle_B)^2}$, with $\langle \dots \rangle_{A(B)}$ being the expectation value at the A (B) sublattice. We note that nonzero $\bar{\tau}^\pm$, $\bar{\rho}^\pm$ indicate the hybridizations of $|0, 1\rangle_{ij} \rightleftharpoons |1, 0\rangle_{ij}$, and $|2, 0\rangle_{ij} \rightleftharpoons |1, 1\rangle_{ij}$, respectively, that are excitonic condensations. Note also that nonzero \bar{n}_k^- , $\bar{\tau}^-$, $\bar{\rho}^-$ indicate a staggered order.

The calculated results are summarized in Fig. 4. Two kinds of exciton condensates actually appear, indicated by

the quantum hybridization of the single-site exciton states. From $h = 0$ to h_{C1} , the spatially uniform $\psi_{\text{vacuum}} = \prod_i |0\rangle_i$ state is the ground state. With a first order transition, the first exciton condensate (EC1) emerges between h_{C1} and h_{C2} , where the magnetic excitonic condensation of the type $\phi_{\text{EC1}} = p_0 |0\rangle + p_1 |1\rangle + p_2 |2\rangle$ appears as indicated by $n_k^+ > 0$ for any k . EC1 is a spatially uniform condensation of single exciton $|1\rangle$ and also of bi-exciton $|2\rangle$, which is indicated by $n_k^- = 0$ for any k . The emergence of EC1 is assisted by the terms $\mathcal{H}_{\text{trans}}$ and $\mathcal{H}_{\text{dual}}$ that induces quantum hybridizations of $|0\rangle$, $|1\rangle$, and $|2\rangle$ states. Next, the second exciton condensate (EC2) emerges between h_{C2} and h_{C3} with a distinct character from EC1, where the A and B sublattices hosts different excitonic states of the type $\phi_{\text{EC2}}^A \simeq q_0 |0\rangle + q_1 |1\rangle$ and $\phi_{\text{EC2}}^B \simeq q'_2 |2\rangle + q'_1 |1\rangle$, respectively. As shown in Fig. 4, n_k^- for $k = 0$ and 2 take large values, suggesting the spatially periodic arrangement of $|0\rangle$ and $|2\rangle$. The superlattice formation coexists with the excitonic condensation in EC2, which thus corresponds to a supersolidity of excitons. The quantum terms $\mathcal{H}_{\text{trans}}$ and $\mathcal{H}_{\text{dual}}$ are indispensable for the appearance of EC1 and EC2, respectively, which are separated by a second-order phase transition. Lastly, above h_{C3} , the saturated phase of $\psi_{\text{Bi-exciton}} = \prod_i |2\rangle_i$ appears due to the largest magnetization and Zeeman energy.

With only the classical terms \mathcal{H}_{loc} and \mathcal{H}_{int} , the phase transitions occur as $\psi_{\text{vacuum}} \leftrightarrow \text{superlattice } |0, 2, 0, 2 \dots\rangle \leftrightarrow \psi_{\text{Bi-exciton}}$ with increasing magnetic fields, as is discussed in Ref. [30]. With the additional quantum effects $\mathcal{H}_{\text{trans}}$ and $\mathcal{H}_{\text{dual}}$, the nontrivial excitonic phases EC1 and EC2 emerge over the classical phases. In fact, EC2 has a root in the classical solid $|0, 2, 0, 2 \dots\rangle$ and the quantum hybridization $\mathcal{H}_{\text{dual}}$. When $t \gg V$, only EC1 appears, and when $t \ll V$, only EC2 appears, on the contrary. When t and V balance, both EC1 and EC2 emerge as a result of the competing energy. We note that the experimentally observed transitions from $\text{LS} \leftrightarrow \beta \leftrightarrow \gamma$ may correspond to the successive phase transitions in the calculated results, $\psi_{\text{vacuum}} \leftrightarrow \text{EC1} \leftrightarrow \text{EC2}$, considering the features that two gapless phases appear in high magnetic fields and that those phases are connected with a continuous phase transition. The correspondence of the two kinds of gapless phases β and γ to EC1 and EC2 infers that considering the duality of the excitons $\mathcal{H}_{\text{dual}}$ and the situation $t \sim V$ may actually be important in LaCoO_3 . See the caption of Fig. 4 and the Supplemental Material for the details of the parameters in the calculation [37]. The negative slope in β may result from the non-trivial spin-lattice coupling found in a high-resolution x-ray diffraction study, where the lattice volume of $|1\rangle$ is claimed to be smaller than a pair of neighboring site $|0\rangle$ and $|2\rangle$ [40]. Increasing the weight of $|1\rangle$ might contract the lattice volume in EC1 with increasing magnetic fields. While, increasing the weight of the alignment with $|0\rangle$ and $|2\rangle$ might expand the lattice volume in EC2. No phase corresponding to α appear in the calculated result. We speculate that α phase emerges with modified interaction parameters by the strong lattice contraction as compared to β phase where the localization nature of excitons is enhanced resulting in exciton superlattice formation

in α phase. Such lattice contraction in the course of β - α phase transition is actually observed in Ref. [18].

We comment on the spin-crossover physics in LaCoO_3 , which has been a long-standing controversy over half a century regarding the temperature evolution of the microscopic understanding of the electronic and magnetic state in terms of the spin-states [41]. As depicted in Fig. 1, there is a correspondence of the exciton occupation states $\{|0\rangle, |1\rangle, |2\rangle\}$ and spin-states $\{\text{LS}, \text{IS}, \text{HS}\}$. HS-LS order have been anticipated by many studies in LaCoO_3 [30, 42]. EC2, that may correspond to β phase, possesses the component of such HS-LS order in the present experiment. Besides, α phase is claimed to originate in a IS-LS superlattice [18]. Recently, the HS-IS duality has been claimed to be at the heart of the controversy over HS and IS states in LaCoO_3 [38, 39], in addition to the delocalization of IS. The delocalization of IS to LS sites, and the HS-IS duality correspond to the itineracy of single exciton and the exciton duality $|2, 0\rangle_{ij} \Leftrightarrow |1, 1\rangle_{ij}$, respectively, that give rise to the exciton condensation EC1 and EC2, respectively. Thus, we argue that the gapless features of β and γ phases may originate in the coherent hybridization of LS-IS-HS states due to the HS-IS duality. Incoherent spin-state hybridizations and superlattices are also argued in Ref. [43]. With an influence of the hybridization effects of LS, IS and HS states, the variety of ordered states of LaCoO_3 at high magnetic fields are realized as shown in Fig. 3(c) and Fig. 4. To fully understand and characterize the possible exciton condensates in β , and γ phases of LaCoO_3 , experimental investigations such as spin transport, neutron scattering and theoretical examinations of more realistic models are mandatory.

* a-ikeda@uec.ac.jp

- [1] N. F. Mott, The transition to the metallic state, *Philos. Mag.* **6**, 287 (1961).
- [2] B. I. Halperin and T. M. Rice, Possible anomalies at a semimetal-semiconductor transition, *Rev. Mod. Phys.* **40**, 755 (1968).
- [3] A. Kogar, M. S. Rak, S. Vig, A. A. Husain, F. Flicker, Y. I. Joe, L. Venema, G. J. MacDougall, T. C. Chiang, E. Fradkin, J. van Wezel, and P. Abbamonte, Signatures of exciton condensation in a transition metal dichalcogenide, *Science* **358**, 1314 (2017).
- [4] Y. F. Lu, H. Kono, T. I. Larkin, A. W. Rost, T. Takayama, A. V. Boris, B. Keimer, and H. Takagi, Zero-gap semiconductor to excitonic insulator transition in Ta_2NiSe_5 , *Nat. Commun.* , 14408 (2017).
- [5] C. W. Lai, N. Y. Kim, S. Utsunomiya, G. Roumpos, H. Deng, M. D. Fraser, T. Byrnes, P. Recher, N. Kumada, T. Fujisawa, and Y. Yamamoto, Coherent zero-state and π -state in an exciton-polariton condensate array, *Nature* **450**, 529 (2007).
- [6] Y. Jia, P. Wang, C.-L. Chiu, Z. Song, G. Yu, B. J'ack, S. Lei, S. Klemen, F. A. Cevallos, M. Onyszczyk, N. Fishchenko, X. Liu, G. Farahi, F. Xie, Y. Xu, K. Watanabe, T. Taniguchi, B. A. Bernevig, R. J. Cava, L. M. Schoop, A. Yazdani, and S. Wu, Evidence for a monolayer excitonic insulator, *Nat. Phys.* **10.1038/s41567-021-01422-w** (2021).
- [7] H. M. Bretscher, P. Andrich, Y. Murakami, D. Golez, B. Remez, P. Telang, A. Singh, L. Harnagea, N. R. Cooper, A. J. Millis,

- P. Werner, A. K. Sood, and A. Rao, Imaging the coherent propagation of collective modes in the excitonic insulator Ta_2NiSe_5 at room temperature, *Sci. Adv.* **7**, eabd6147 (2021).
- [8] W. Yuan, Q. Zhu, T. Su, Y. Yao, W. Xing, Y. Chen, Y. Ma, X. Lin, J. Shi, R. Shindou, X. C. Xie, and W. Han, Experimental signatures of spin superfluid ground state in canted antiferromagnet Cr_2O_3 via nonlocal spin transport, *Sci. Adv.* **4**, eaat1098 (2018).
- [9] Z. Jiang, W. Lou, Y. Liu, Y. Li, H. Song, K. Chang, W. Duan, and S. Zhang, Spin-Triplet Excitonic Insulator: The Case of Semihydrogenated Graphene, *Phys. Rev. Lett.* **124**, 166401 (2020).
- [10] J. Nasu and M. Naka, Spin seebeck effect in nonmagnetic excitonic insulators, *Phys. Rev. B* **103**, L121104 (2021).
- [11] T. Kaneko, B. Zenker, H. Fehske, and Y. Ohta, Competition between excitonic charge and spin density waves: Influence of electron-phonon and Hund's rule couplings, *Phys. Rev. B* **92**, 115106 (2015).
- [12] J. Kuneš, Excitonic condensation in systems of strongly correlated electrons, *J. Phys. Cond. Mat.* **27**, 333201 (2015).
- [13] J. Nasu, T. Watanabe, M. Naka, and S. Ishihara, Phase diagram and collective excitations in an excitonic insulator from an orbital physics viewpoint, *Phys. Rev. B* **93**, 205136 (2016).
- [14] A. Sotnikov and J. Kuneš, Field-induced exciton condensation in LaCoO_3 , *Sci. Rep.* **6**, 30510 (2016).
- [15] T. Tatsuno, E. Mizoguchi, J. Nasu, M. Naka, and S. Ishihara, Magnetic field effects in a correlated electron system with spin-state degree of freedom — implications for an excitonic insulator —, *J. Phys. Soc. Jpn.* **85**, 083706 (2016).
- [16] D. Nakamura, A. Ikeda, H. Sawabe, Y. H. Matsuda, and S. Takeyama, Record indoor magnetic field of 1200 T generated by electromagnetic flux-compression, *Rev. Sci. Instrum.* **89**, 095106 (2018).
- [17] A. Ikeda, T. Nomura, Y. H. Matsuda, S. Tani, Y. Kobayashi, H. Watanabe, and K. Sato, High-speed 100 MHz strain monitor using fiber Bragg grating and optical filter for magnetostriction measurements under ultrahigh magnetic fields, *Rev. Sci. Instrum.* **88**, 083906 (2017).
- [18] A. Ikeda, Y. H. Matsuda, and K. Sato, Two spin-state crystallizations in LaCoO_3 , *Phys. Rev. Lett.* **125**, 177202 (2020).
- [19] A. Ikeda, T. Nomura, Y. H. Matsuda, A. Matsuo, K. Kindo, and K. Sato, Spin state ordering of strongly correlating LaCoO_3 induced at ultrahigh magnetic fields, *Phys. Rev. B* **93**, 220401(R) (2016).
- [20] M. Manago, S. Kitagawa, K. Ishida, K. Deguchi, N. K. Sato, and T. Yamamura, Spin-triplet superconductivity in the paramagnetic UCoGe under pressure studied by ^{59}Co NMR, *Phys. Rev. B* **100**, 035203 (2019).
- [21] S. Ran, C. Eckberg, Q. P. Ding, Y. Furukawa, T. Metz, S. R. Saha, I. L. Liu, M. Zic, H. Kim, J. Paglione, and N. P. Butch, Nearly ferromagnetic spin-triplet superconductivity, *Science* **365**, 684 (2019).
- [22] W. P. Halperin, Superfluid ^3He in Aerogel, *Annu. Rev. Condens. Matter Phys.* **10**, 155 (2019).
- [23] T. Kaneko and Y. Ohta, Electric and magnetic multipoles and bond orders in excitonic insulators, *Phys. Rev. B* **94**, 125127 (2016).
- [24] J. Hejtmanek, Z. Jiráček, O. Kaman, K. Knížek, E. Šantavá, K. Nitta, T. Naito, and H. Fujishiro, Phase transition in $\text{Pr}_{0.5}\text{Ca}_{0.5}\text{CoO}_3$ and related cobaltites, *Eur. Phys. J. B* **86**, 305 (2013).
- [25] J. Kuneš and P. Augustinský, Excitonic instability at the spin-state transition in the two-band hubbard model, *Phys. Rev. B* **89**, 115134 (2014).
- [26] A. Sotnikov and J. Kuneš, Competing phases in a model of Pr-based cobaltites, *Phys. Rev. B* **96**, 245102 (2017).
- [27] T. M. Rice, Quantum mechanics. To condense or not to condense, *Science* **298**, 760 (2002).
- [28] V. Zapf, M. Jaime, and C. U. Batista, Bose-Einstein condensation in quantum magnets, *Rev. Mod. Phys.* **86**, 563 (2014).
- [29] K. Sato, A. Matsuo, K. Kindo, Y. Kobayashi, and K. Asai, Field induced spin-state transition in LaCoO_3 , *J. Phys. Soc. Jpn.* **78**, 093702 (2009).
- [30] M. M. Altarawneh, G. W. Chern, N. Harrison, C. D. Batista, A. Uchida, M. Jaime, D. G. Rickel, S. A. Crooker, C. H. Mielke, J. B. Betts, J. F. Mitchell, and M. J. R. Hoch, Cascade of magnetic field induced spin transitions in LaCoO_3 , *Phys. Rev. Lett.* **109**, 037201 (2012).
- [31] M. Rotter, Z. S. Wang, A. T. Boothroyd, D. Prabhakaran, A. Tanaka, and M. Doerr, Mechanism of spin crossover in LaCoO_3 resolved by shape magnetostriction in pulsed magnetic fields, *Sci. Rep.* **4**, 7003 (2014).
- [32] R. Schönemann, G. Rodriguez, D. Rickel, F. Balakirev, R. D. McDonald, J. A. Evans, B. Maiorov, C. Paillard, L. Bellaiche, A. V. Stier, M. B. Salamon, K. Gofryk, and M. Jaime, Magnetoelastic standing waves induced in UO_2 by microsecond magnetic field pulses, *Proc. Natl. Acad. Sci. U. S. A.* **118**, e2110555118 (2021).
- [33] (), see section I in the Supplemental Material.
- [34] T. Kyömen, Y. Asaka, and M. Itoh, Negative cooperative effect on the spin-state excitation in LaCoO_3 , *Phys. Rev. B* **67**, 144424 (2003).
- [35] T. Kihara, Y. Kohama, M. Tokunaga, and K. Sato, Unpublished.
- [36] S. Noguchi, S. Kawamata, K. Okuda, H. Nojiri, and M. Motokawa, Evidence for the excited triplet of LaCoO_3 , *Phys. Rev. B* **66**, 094404 (2002).
- [37] (), see section II in the Supplemental Material.
- [38] K. Tomiyasu, T. Nomura, Y. Kobayashi, S. Ishihara, S. Ohira, and M. Kofu, Emergent units of itinerant spin-state excitations in LaCoO_3 , *arXiv:1808.05888*.
- [39] A. Hariki, R.-P. Wang, A. Sotnikov, K. Tomiyasu, D. Betto, N. B. Brookes, Y. Uemura, M. Ghiasi, F. M. F. d. Groot, and J. Kuněš, Melting of excitonic dispersion in LaCoO_3 : theory and experiment, *Phys. Rev. B* **101**, 245162 (2020).
- [40] P. G. Radaelli and S. W. Cheong, Structural phenomena associated with the spin-state transition in LaCoO_3 , *Phys. Rev. B* **66**, 094408 (2002).
- [41] Y. Okimoto, T. Saitoh, Y. Kobayashi, and S. Ishihara, eds., *Spin-Crossover Cobaltite (Review and Outlook)*, Springer Series in Materials Science (Springer Singapore, 2021).
- [42] P. M. Raccach and J. B. Goodenough, First-Order Localized-Electron \rightleftharpoons Collective-Electron Transition in LaCoO_3 , *Phys. Rev.* **155**, 932 (1967).
- [43] K. Knížek, Z. Jiráček, J. Hejtmanek, P. Novák, and W. Ku. Gga+u calculations of correlated spin excitations in LaCoO_3 , *Phys. Rev. B* **79**, 014430 (2009).

Methods The magnetic fields up to 600 T are generated using electromagnetic flux compression method [16] in the Institute for Solid State Physics, the University of Tokyo, Japan. The magnetostriction measurement is performed using our state-of-the-art high-speed strain gauge utilizing fiber Bragg grating and optical filter method [17]. Polycrystalline samples of LaCoO_3 were prepared by the solid-state-reaction of predried La_2O_3 and CoO at 1300 C° in air. The sample is cut out in $1 \times 3 \times 0.5$ mm. FBG fiber is glued tightly onto a specimen of the sample using Stycast 1266. See Supplemental Material for details [33].

Acknowledgements The work is financially supported by JSPS KAKENHI Grant-in-Aid for Early-Career Scientists Grant No. 18K13493 and Basic Science Program No. 18-001 of Tokyo Electric Power Company (TEPCO) memorial foundation.

Author contributions A.I. designed the research. S.K prepared the sample. A.I., Y.H.M., H.S., D.N., S.T. performed the experiments. A.I. analysed the data. J.N. and A.I. developed the model. J.N. performed the calculations. A.I. Y.H.M., J.N. discussed the results. A.I. wrote the manuscript with input from all co-authors.

Competing interests The authors declare no competing interests.

Supplemental material:

Akihiko Ikeda,^{1,2} Yasuhiro H. Matsuda,¹ Keisuke Sato,³ Yuto Ishii,¹

Hironobu Sawabe,¹ Daisuke Nakamura,¹ Shojiro Takeyama,¹ and Joji Nasu^{4,5}

¹*Institute for Solid State Physics, University of Tokyo, Kashiwa, Chiba 277-8581, Japan*

²*Department of Engineering Science,*

University of Electro-Communications, Chofu, Tokyo 182-8585, Japan

³*National Institute of Technology, Ibaraki College,*

Hitachinaka, Ibaraki 312-0011, Japan

⁴*Department of Physics, Tohoku University, Sendai, Miyagi 980-8578, Japan*

⁵*PRESTO, Japan Science and Technology Agency,*

Honcho Kawaguchi, Saitama 332-0012, Japan

(Dated: January 11, 2022)

I. EXPERIMENTAL DETAILS

A. Generation of 600 T using electromagnetic flux compression method in ISSP

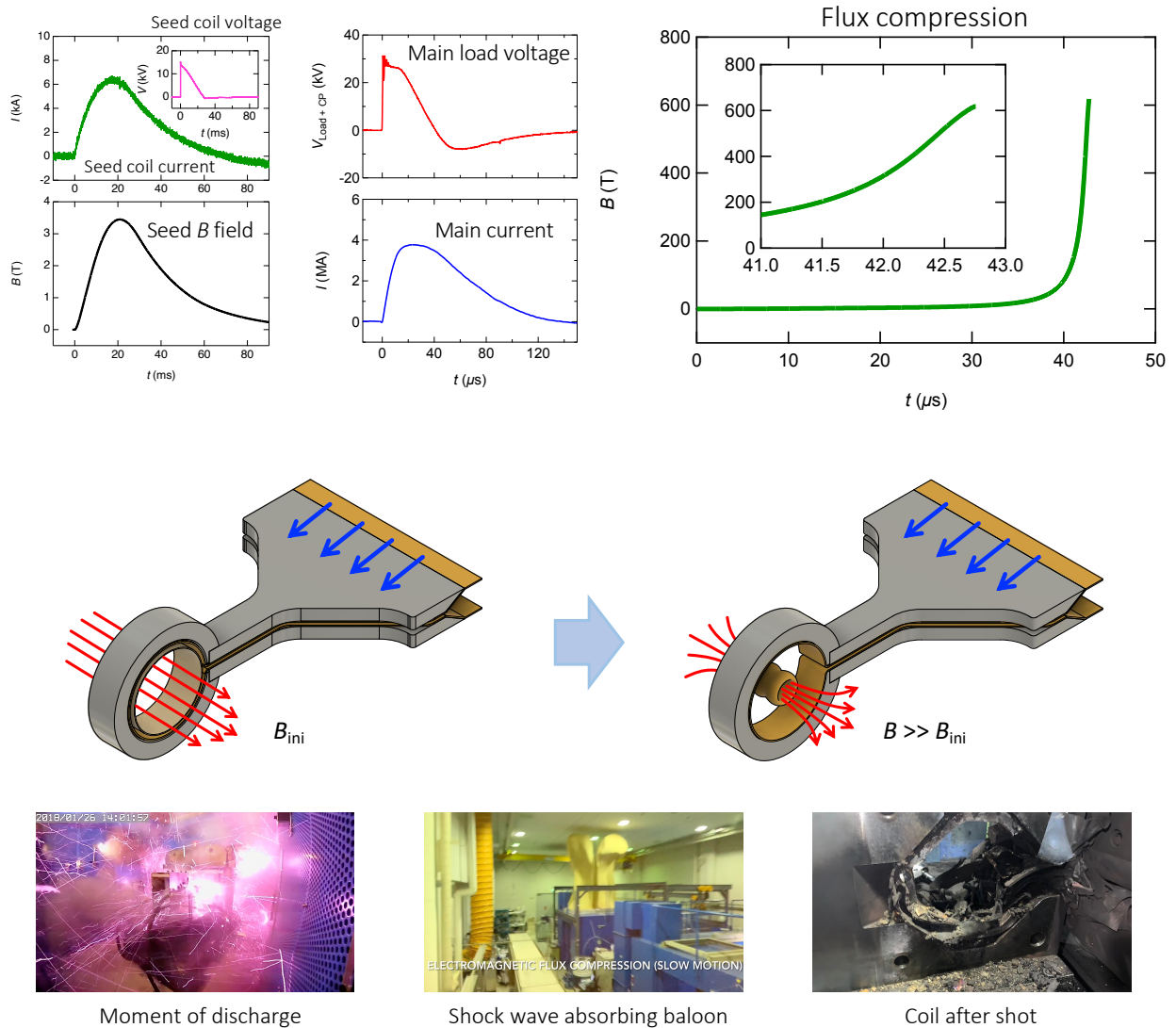


FIG. S1. The seed field generation and the main current used for the flux compression, and the typical magnetic field waveform in the present EMFC experiments.

Electromagnetic flux compression (EMFC) method is used to generate an ultrahigh magnetic field of 600 T in ISSP, University of Tokyo, that we implemented recently [1]. In the EMFC method, the ultrahigh magnetic field is generated by concentrating the seed magnetic flux into a small cross-section and volume. A cylindrical metallic liner is rapidly compressed using the electromagnetic force for the flux concentration. The electromagnetic force orig-

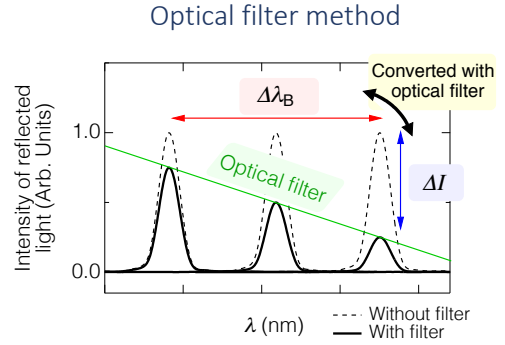
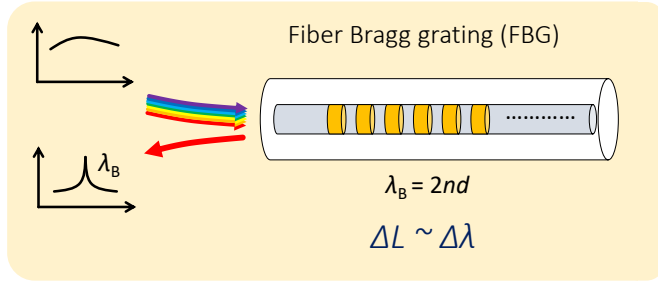


FIG. S2. Schematic drawing of principle of FBG strain gauge and optical filter method for 100 MHz high speed detection of strain.

inates in the current repulsion between the main coil and the induced current inside the metallic liner. A Helmholtz coil is used to generate seed magnetic field of 3.4 T, where the energy stored in the sub capacitor bank is 0.95 MJ at a charging voltage of 13.8 kV. Peak current of the main coil is 3.8 MA discharged with a charging voltage of 40 kV, where the energy stored in the main capacitor bank is 2.56 MJ. In Figs. S1, the waveform of the seed magnetic field, main current and magnetic field are shown along with the schematic drawing of the flux compression and the pictures of the EMFC experiment in ISSP.

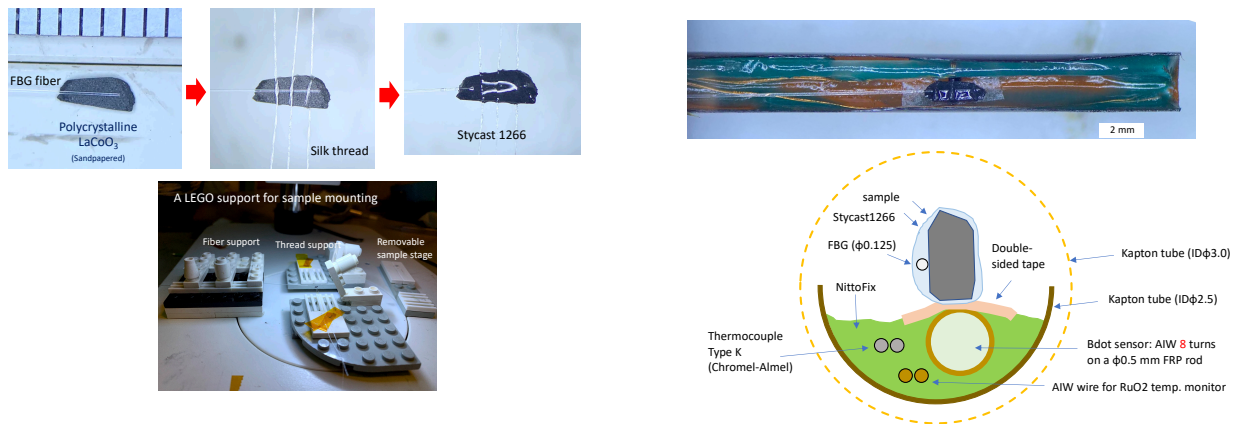


FIG. S3. Technique for gluing the sample and FBG fiber together using silk thread. A LEGO(R) support was used. The picture and the schematic cross-section of the sample probe are shown.

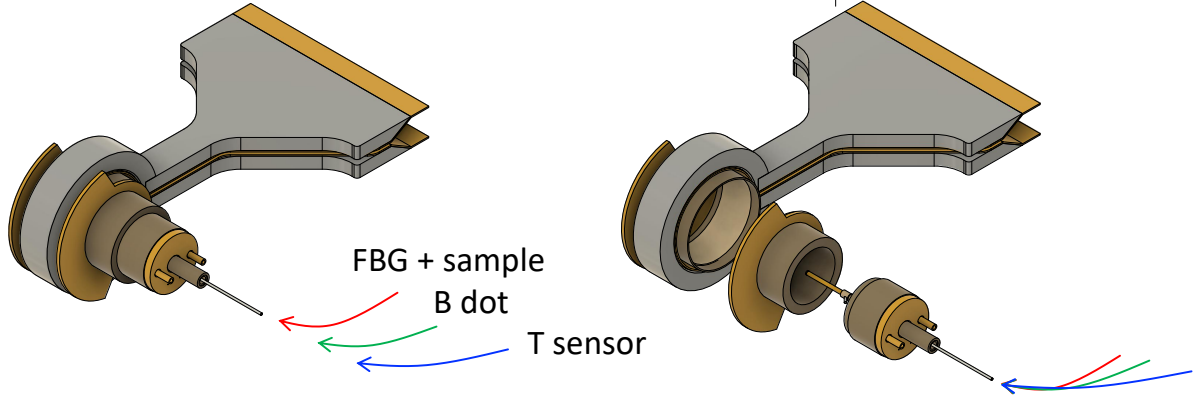


FIG. S4. The image of the vacuum chamber and the cryostat for the EMFC experiments. The sample and all the sensors are inserted from the right end of the image, being removable from the system.

B. High-speed magnetostriction measurement using fiber Bragg grating and optical filter method for the use up to 600 T

We have employed the original high-speed strain gauge utilizing fiber Bragg grating (FBG) technique and optical filter method [2, 3] to measure the longitudinal magnetostriction of LaCoO_3 under ultrahigh magnetic fields generated using EMFC. Requirements for the magnetostriction measurement with EMFC are 100 MHz high speed and noiselessness. FBG is an optical fiber equipped with optical Bragg grating in the core, that we can use as an optical strain gauge as schematically shown in Fig. S2. The strain of the optical fiber is sensitively appears as the shift of the Bragg wavelength. Thus, the shift of the Bragg wavelength can be monitored optically from a distance, which is of a benefit considering a large noise from the explosion and electric discharge involved in EMFC technique. We used the optical filter method as the detection scheme [2]. This is because the required measurement speed is as high as 100 MHz in the EMFC experiment. In the optical filter method, the shift of the Bragg wavelength is converted to the change of the intensity of the optical signal as schematically shown in Fig. S2. The change of the intensity of the optical signal is monitored by the InGaAs avalanche photodiode.

The strain of the sample is transmitted to the FBG fiber that is glued together [See Fig. S3]. The glueing has been carried out in the following manner. First, two or three silk

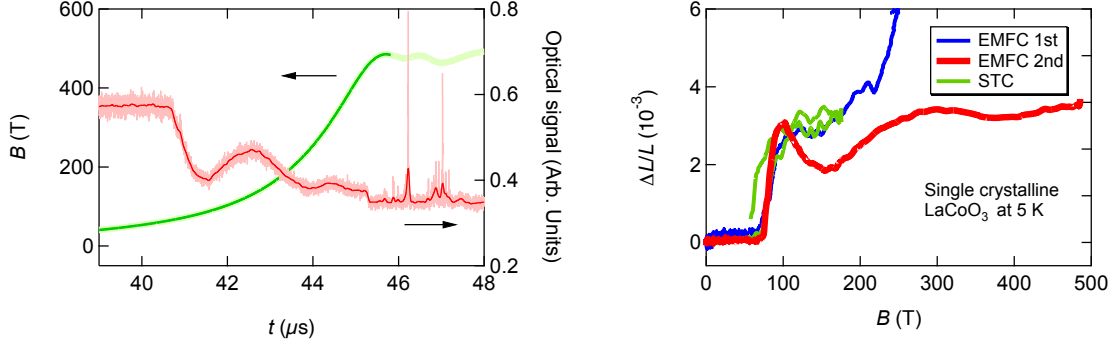


FIG. S5. Results of magnetostriction measurement using single crystalline LaCoO_3 up to 600 T at 5 K.

threads are used to tie the sample to the FBG fiber. This is performed on the base made from LEGO(R) bricks. The bottom base is removed and STYCAST 1266 is used to glue the sample and the FBG fiber with the silk thread. The silk thread is used to make sure the FBG fiber is intact with the sample during the drying process. The glueing method is the heart of the technique. The glued sample and FBG are placed on a Kapton sample holder tube. The induction type magnetic field sensor and temperature monitors of thermocouple or resistive RuO_2 tip are placed nearby in a diameter of ϕ 2.5 mm [See Fig. S3]. The probe equipped with the sample, FBG strain gauge, magnetic field sensor, and the temperature sensors are inserted into a He flow type cryostat. The cryostat is placed at the field center inside a vacuum chamber made of bakelite parts, which serve as a thermal insulator and is also advantageous for the Cu liner implosion in EMFC technique [See Fig. S4].

C. Magnetostriction measurements with single crystalline samples

Single crystalline samples are measured up to 200 T as shown in Fig. S5. It is difficult to observe the temperature dependence coherently with many pulses because single crystalline samples break themselves due to the field induced phase transition taking place too rapidly. The strong vibrations of the data are present [See Fig. S5]. The temperature dependent data is disturbed and incomparable due to the re-gluing fresh samples to new optical fibers. On the other hand, polycrystalline samples are robust against the spin-state transitions triggered by the rapid magnetic field pulse. Poly- and single-crystalline samples show basically identical results with a minor difference in the sharpness of the spin-state transitions.

D. Consideration on spin-orbit interactions

An influence of spin-orbit interaction may result in a slope in magnetostriction. Previously, we argued that the magnetization increases with increasing magnetic fields in β phase although magnetostriction is a constant, which may induce the spin driven lattice change through spin-orbit coupling. We confirmed that this is not the case with measurements of magnetostriction and magnetization at room temperature, where only magnetization increases up to 50 T without any increase in magnetostriction [3]. It is reasonable to assume that the spin-orbit coupling, a local interaction, is temperature independent and is also absent at 78 and 108 K. This justifies our assumption that the longitudinal magnetostriction is proportional lattice volume in the present study. The influence of orbital order is also unlikely either because we presently used a polycrystalline sample.

II. MEAN FIELD CALCULATION

Next, we present the details of the theoretical model for the magnetic properties of trivalent cobalt ions ($3d^6$) in LaCoO_3 in an applied magnetic field and introduce the calculation method to address the model.

A. Model

We start from the five-orbital Hubbard model under the magnetic field to understand the properties of $3d$ electrons in cobalt ions. This model is composed of the following four terms: the transfer integrals between $3d$ orbitals in neighboring ions, \mathcal{H}_t , on-site Coulomb interactions \mathcal{H}_U , crystalline electric field $\mathcal{H}_{\text{crys}}$ with the octahedral symmetry, and Zeeman term \mathcal{H}_Z . Since there are five orbitals, which are occupied by six electrons per site, the Hamiltonian is extremely complicated. The competition between the local Hamiltonians, \mathcal{H}_U and $\mathcal{H}_{\text{crys}}$, is understood from the well-known Tanabe-Sugano diagram. In the d^6 configurations, three types of spin states, low-spin (LS), intermediate spin (IS), and high-spin states (HS) shown in Fig. S6 play a crucial role in the magnetic properties of a local cobalt site. When the on-site Coulomb interactions are only taken into account, the ground state of the local d^6 configurations is the LS multiplet 5D ($S = 2, L = 2$) corresponding to the HS state while the IS and LS are excited states. By introducing the crystalline electric field

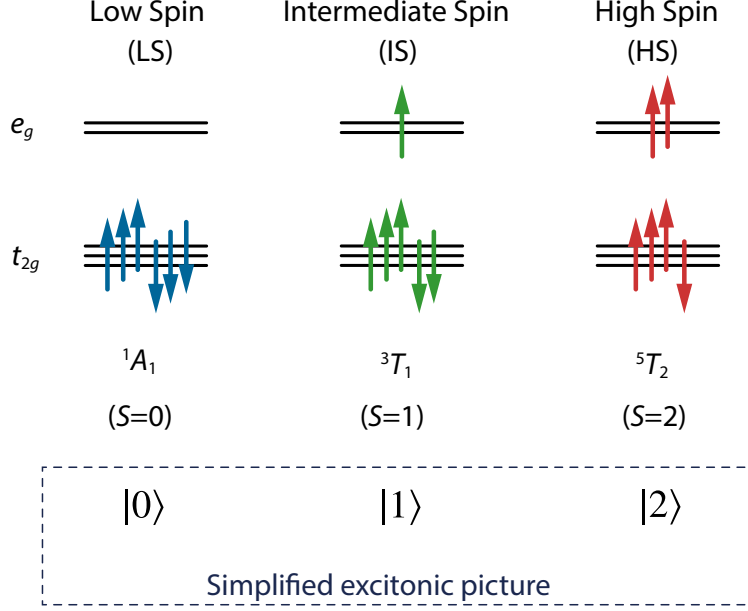


FIG. S6. Schematic picture of the three spin states and their excitonic representations simplified in the magnetic field.

of the octahedral ligand arrangement, the ground state changes to the LS state where the t_{2g} orbitals are fully occupied. The IS can be a first excited state but does not become a ground state within a single ion system. Nevertheless, intensive experimental and theoretical studies on cobalt oxides suggested the possibility of the emergence of the IS state due to the competition between itinerant and localized natures of electrons.

Next, we discuss the effect of the Zeeman term \mathcal{H}_Z . The strong magnetic field lifts spin and orbital degeneracies, which allows us to extract a state with the Zeeman energy minimized in each spin-state manifold. Such states in LS, IS, and HS manifold are referred to as $|0\rangle$, $|1\rangle$, and $|2\rangle$, respectively. Here, we neglect the degeneracy surviving under the magnetic field in each spin state for simplicity. We construct the low-energy effective Hamiltonian in the subspace composed of the direct products of the three local states $|0\rangle$, $|1\rangle$, and $|2\rangle$ in the strong correlation limit. The effective Hamiltonian is written as

$$\mathcal{H} = \mathcal{H}_{\text{loc}} + \mathcal{H}_{\text{int}} + \mathcal{H}_{\text{trans}} + \mathcal{H}_{\text{dual}}. \quad (\text{S1})$$

The first term \mathcal{H}_{loc} represents the local energy levels of the IS and HS states, which is given

by

$$\mathcal{H}_{\text{loc}} = (E_1 - g_1 h) \sum_i n_i^{(1)} + (E_2 - g_2 h) \sum_i n_i^{(2)}, \quad (\text{S2})$$

where E_1 and E_2 are the on-site energies of $|1\rangle$ and $|2\rangle$ measured from the LS one, respectively, and $n_i^{(1)} = |1\rangle_i \langle 1|_i$ and $n_i^{(2)} = |2\rangle_i \langle 2|_i$ are the number operators at site i . The g factors for the IS and HS states are written as $g_1 = 1$ and $g_2 = 2$ under the magnetic field h . E_1 and E_2 should be positive because the ground state without magnetic fields is LS state.

The other terms in Eq. (S1) are deduced from the second-order perturbation process with respect to \mathcal{H}_t . For simplicity, we neglect the orbital anisotropy related to bond-dependent transfer integrals in \mathcal{H}_t . First, we consider the diagonal part, where a local spin state is not changed by the perturbation process. The transfer integrals between the e_g orbitals at neighboring sites is much larger than those involving the t_{2g} orbitals when the neighboring octahedra share their corners. In this case, the energy gain is yielded by the perturbation process for the IS-IS, LS-HS, LS-IS, and IS-HS configurations at neighboring sites. While the IS state does not become the ground state in a single ion system, one expects more perturbation processes involving the IS state than the HS because of the orbital degeneracy of the e_g orbitals in the IS state. Thus, we extract the IS-IS and LS-HS configurations as dominant contributions, and the corresponding Hamiltonian is given by

$$\mathcal{H}_{\text{int}} = -J_{11} \sum_{\langle ij \rangle} n_i^{(1)} n_j^{(1)} - J_{02} \sum_{\langle ij \rangle} (n_i^{(2)} n_j^{(0)} + n_i^{(0)} n_j^{(2)}), \quad (\text{S3})$$

where $n_i^{(0)}$ is the number operator for the LS state. Note that J_{11} and J_{02} should be positive because of the second-order perturbation.

Next, we consider the exchange terms in the perturbation expansion. As suggested in Ref. 4, there are two dominant processes: the exchange process between neighboring LS and IS states and the change from the neighboring two IS states into LS and HS states. The former is interpreted as the hopping of a single exciton to a neighboring site, $|0, 1\rangle_{ij} \rightleftharpoons |1, 0\rangle_{ij}$, and latter as the fusion of two single excitons into a bi-exciton (and the fission of it), $|1, 1\rangle_{ij} \rightleftharpoons |0, 2\rangle_{ij}$. These contributions are given by

$$\mathcal{H}_{\text{trans}} = -t \sum_{\langle ij \rangle} \left(|0, 1\rangle_{ij} \langle 1, 0|_{ij} + |1, 0\rangle_{ij} \langle 0, 1|_{ij} \right), \quad (\text{S4})$$

$$\mathcal{H}_{\text{dual}} = -V \sum_{\langle ij \rangle} \left[|1, 1\rangle_{ij} \left(\langle 2, 0|_{ij} + \langle 0, 2|_{ij} \right) + \left(|2, 0\rangle_{ij} + |0, 2\rangle_{ij} \right) \langle 1, 1|_{ij} \right], \quad (\text{S5})$$

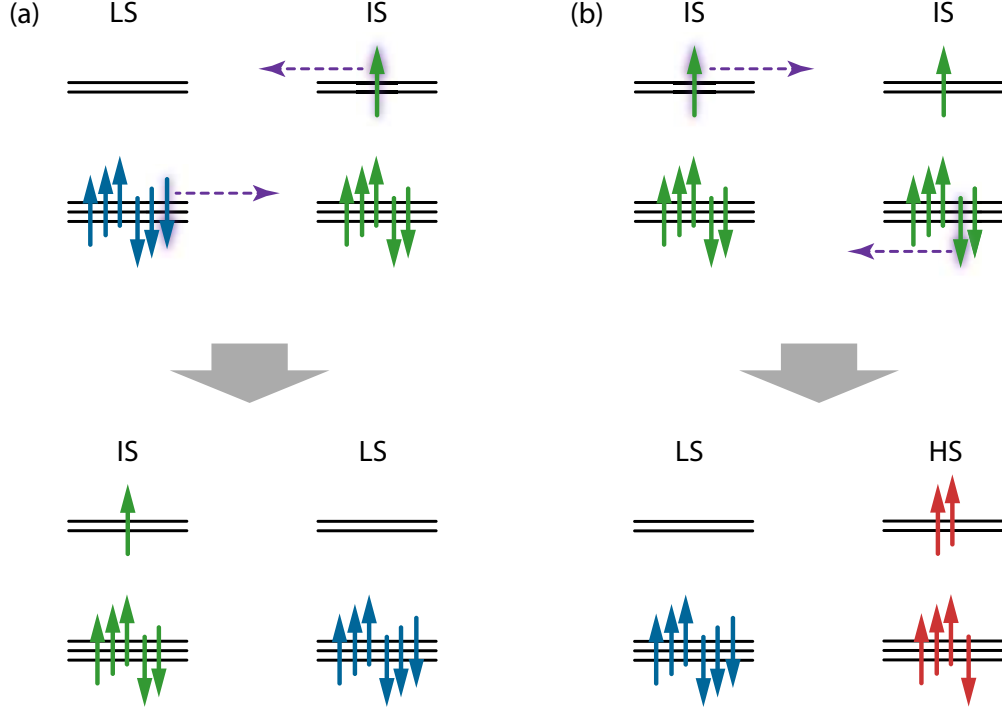


FIG. S7. Two types of second-order perturbation processes changing neighboring local spin states: (a) the exchange process between LS and IS states and (b) the process where two IS states are changed to LS and HS states, which is regarded as a fusion process of two single-excitons to a bi-exciton.

where $|k, k'\rangle_{ij} = |k\rangle_i \otimes |k'\rangle_j$.

The exchange constants, E_1 , E_2 , J_{11} , J_{02} , t , and V should be obtained from the perturbation procedure, but determining their values is a significantly tough problem. To avoid this, we regard these constants as external parameters. The signs of t and V cannot be determined directly. Fortunately, these can be inverted by an appropriate gauge transformation in the case of the bipartite lattice. Here, we consider the three-dimensional cubic lattice with the coordination number $z = 6$. In this case, the obtained phase diagram does not depend on the signs. Thus, we assume that t and V are positive hereafter.

B. Mean-field theory

Here, we show the details of the mean-field theory applied to the model Hamiltonian given in Eq. (S1). We introduce two types of pseudospins, τ_i and ρ_i at site i , which are

defined by

$$\tau_i^x = |0\rangle_i \langle 1|_i + \text{H.c.}, \quad \tau_i^y = i |0\rangle_i \langle 1|_i + \text{H.c.}, \quad (\text{S6})$$

$$\rho_i^x = |1\rangle_i \langle 2|_i + \text{H.c.}, \quad \rho_i^y = i |1\rangle_i \langle 2|_i + \text{H.c.}, \quad (\text{S7})$$

respectively. Using these pseudospins, $\mathcal{H}_{\text{trans}}$ and $\mathcal{H}_{\text{dual}}$ are rewritten as

$$\mathcal{H}_{\text{trans}} = -\frac{t}{2} \sum_{\langle ij \rangle} (\tau_i^x \tau_j^x + \tau_i^y \tau_j^y), \quad (\text{S8})$$

$$\mathcal{H}_{\text{dual}} = -\frac{V}{2} \sum_{\langle ij \rangle} (\tau_i^x \rho_j^x + \rho_i^x \tau_j^x + \tau_i^y \rho_j^y + \rho_i^y \tau_j^y). \quad (\text{S9})$$

We apply the mean-field decoupling to \mathcal{H}_{int} , $\mathcal{H}_{\text{trans}}$, and $\mathcal{H}_{\text{dual}}$, where two-sublattice orders are assumed. The order parameters are given by $\langle \tau^x \rangle_X$, $\langle \tau^y \rangle_X$, $\langle \rho^x \rangle_X$, $\langle \rho^y \rangle_X$, and $\langle n^k \rangle_X$, where $k = 0, 1, 2$ and $X (= A, B)$ is the sublattice index. The operator $\boldsymbol{\tau}$ corresponds to a mixing between the LS and IS states, and a nonzero $\langle \boldsymbol{\tau} \rangle_X$ suggests excitonic condensation, while a nonzero expectation value of the operator $\boldsymbol{\rho}$ indicates a spontaneous hybridization between IS and HS states. Note that the U(1) symmetry appears to be present in $\mathcal{H}_{\text{trans}}$ in the pseudospin space but it is due to the simplification of the effective model. If we carry out a more rigorous derivation of the effective model from the multi-orbital Hubbard model, this symmetry should be absent in the obtained Hamiltonian [5].

C. Mean-field result

We show the results of mean-field calculations for the effective model given in Eq. (S1). Figure S8 shows the magnetic-field dependence of the mean-field energy, classical energies given by

$$\begin{cases} E_0 = 0, \\ E_{11} = E_1 - g_1 h - z J_{11}/2, \\ E_{22} = E_2 - g_2 h, \\ E_{02} = (E_2 - g_2 h - z J_{02})/2, \end{cases} \quad (\text{S10})$$

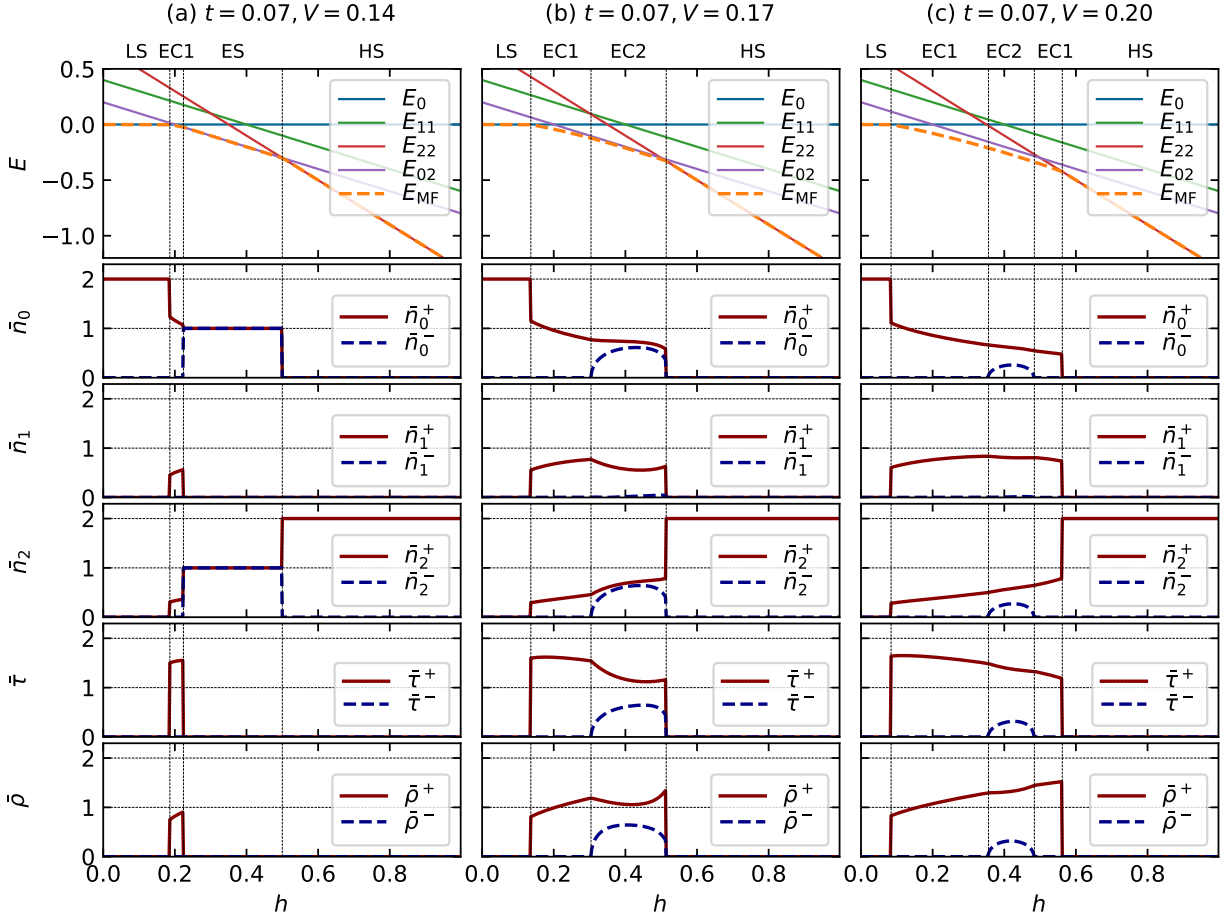


FIG. S8. Mean-field results for the effective model given in Eq. (S1) at (a) $V = 0.14$, (b) $V = 0.17$, and (c) $V = 0.20$. The other parameters are chosen to be $(E_1, E_2, J_{11}, J_{02}, t) = (1.0, 0.7, 0.2, 0.05, 0.07)$. The top panels represent the mean-field energy and classical energies given in Eq. (S10) as functions of h . The others show the field dependence of the mean-fields given in Eq. (S11). The energy unit in the present calculations is E_1 , which is estimated as ~ 10 meV corresponding to ~ 100 T.

and the order parameters given by

$$\begin{cases}
 \bar{n}_k^\pm = |\langle n^{(k)} \rangle_A \pm \langle n^{(k)} \rangle_B|, & (k = 0, 1, 2) \\
 \bar{\tau}^\pm = \sqrt{(\langle \tau^x \rangle_A \pm \langle \tau^x \rangle_B)^2 + (\langle \tau^y \rangle_A \pm \langle \tau^y \rangle_B)^2}, \\
 \bar{\rho}^\pm = \sqrt{(\langle \rho^x \rangle_A \pm \langle \rho^x \rangle_B)^2 + (\langle \rho^y \rangle_A \pm \langle \rho^y \rangle_B)^2}.
 \end{cases} \quad (\text{S11})$$

We choose the parameters in Eq. (S1) such that the LS is realized in the ground state in the absence of the magnetic field and this state changes to the LS-HS order and uniform

HS state successively by applying the magnetic field in the classical case where $\mathcal{H}_{\text{trans}}$ and $\mathcal{H}_{\text{dual}}$ are dropped. The LS-HS order is regarded as the exciton solid (ES). The previous experimental studies suggest the situation [3, 6, 7], and thereby, we focus on the parameters shown in Fig. S8, which satisfy the above conditions.

The parameters in Fig. S8(b) is the same as those of the mean-field result shown in the main text. In this case, we find two excitonic phases, EC1 and EC2, in addition to the uniform LS and HS phases. The EC1 state is characterized by the uniform excitonic order parameters $\bar{\tau}^+$ and $\bar{\rho}^+$. Since \bar{n}_2 is smaller than \bar{n}_0 and \bar{n}_1 , this state is interpreted as condensation of single-excitons [1]. On the other hand, in the EC2 state, the staggered component of the order parameters continuously appears from the EC1 phase, indicating the second-order phase transition between EC1 and EC2. Among them, \bar{n}_1^- is much smaller than the others, which suggests that the solidification of bi-excitons emerges together with excitonic condensation. Thus, the EC2 is regarded as an excitonic supersolid. This phase is shrunk with increasing V as shown in Fig. S8(c). On the other hand, Fig. S8(a) indicates that the decrease of V changes the EC2 to the classical ES state. In this case, the phase transition between EC1 and ES is of first order. Therefore, we deduce that the fusion of the two single-excitons, caused by $\mathcal{H}_{\text{dual}}$, play a crucial role in inducing the EC2 state and the second-order transition to the EC1.

-
- [1] D. Nakamura, A. Ikeda, H. Sawabe, Y. H. Matsuda, and S. Takeyama, [Rev. Sci. Instrum.](#) **89**, 095106 (2018).
 - [2] A. Ikeda, T. Nomura, Y. H. Matsuda, S. Tani, Y. Kobayashi, H. Watanabe, and K. Sato, [Rev. Sci. Instrum.](#) **88**, 083906 (2017).
 - [3] A. Ikeda, Y. H. Matsuda, and K. Sato, [Phys. Rev. Lett.](#) **125**, 177202 (2020).
 - [4] A. Hariki, R.-P. Wang, A. Sotnikov, K. Tomiyasu, D. Betto, N. B. Brookes, Y. Uemura, M. Ghiasi, F. M. F. d. Groot, and J. Kuněs, [Phys. Rev. B](#) **101**, 245162 (2020).
 - [5] J. Nasu, T. Watanabe, M. Naka, and S. Ishihara, [Phys. Rev. B](#) **93**, 205136 (2016).
 - [6] M. M. Altarawneh, G. W. Chern, N. Harrison, C. D. Batista, A. Uchida, M. Jaime, D. G. Rickel, S. A. Crooker, C. H. Mielke, J. B. Betts, J. F. Mitchell, and M. J. R. Hoch, [Phys. Rev. Lett.](#) **109**, 037201 (2012).

- [7] A. Ikeda, T. Nomura, Y. H. Matsuda, A. Matsuo, K. Kindo, and K. Sato, [Phys. Rev. B **93**, 220401\(R\) \(2016\)](#).